



The Maternal Microbiome Programs the m⁶A Epitranscriptome of the Mouse Fetal Brain and Intestine

Zhuoyu Xiao^{1†}, Sun Liu^{1†}, Zengguang Li^{1†}, Jinru Cui¹, Hailan Wang¹, Zihan Wang¹, Qihuan Ren¹, Laixin Xia^{1*}, Zhijian Wang^{2*} and Yuan Li^{1*}

¹Department of Developmental Biology, School of Basic Medical Sciences, Southern Medical University, Guangzhou, China,

²Department of Obstetrics and Gynecology, Nanfang Hospital, Southern Medical University, Guangzhou, China

OPEN ACCESS

Edited by:

Huilin Huang,
Sun Yat-sen University Cancer Center
(SYSUCC), China

Reviewed by:

Huizhe Wu,
China Medical University, China
Pengze Yan,
Dana-Farber Cancer Institute,
United States
Yu Hou,
Chongqing Medical University, China

*Correspondence:

Laixin Xia
xialx@smu.edu.cn
Zhijian Wang
wzjnfyy@163.com
Yuan Li
gavin@smu.edu.cn

[†]These authors have contributed
equally to this work

Specialty section:

This article was submitted to
Epigenomics and Epigenetics,
a section of the journal
Frontiers in Cell and Developmental
Biology

Received: 24 February 2022

Accepted: 06 June 2022

Published: 07 July 2022

Citation:

Xiao Z, Liu S, Li Z, Cui J, Wang H,
Wang Z, Ren Q, Xia L, Wang Z and Li Y
(2022) The Maternal Microbiome
Programs the m⁶A Epitranscriptome of
the Mouse Fetal Brain and Intestine.
Front. Cell Dev. Biol. 10:882994.
doi: 10.3389/fcell.2022.882994

The microbiome exerts profound effects on fetal development and health, yet the mechanisms underlying remain elusive. N6-methyladenosine (m⁶A) plays important roles in developmental regulation. Although it has been shown that the microbiome affects the mRNA m⁶A modification of the host, it remains unclear whether the maternal microbiome affects m⁶A epitranscriptome of the fetus so as to impact fetal development. Here, we found that loss of the maternal microbiome altered the expression of m⁶A writers and erasers, as well as the m⁶A methylome of the mouse fetal brain and intestine on embryonic day 18. From the m⁶A profiles, we identified 2,655 and 2,252 m⁶A modifications regulated by the maternal microbiome in the fetal brain and intestine, respectively, and we demonstrated that these m⁶A-modified genes were enriched in the neuro/intestinal developmental pathways, such as the Wnt signaling pathway. Finally, we verified that antibiotic treatment mostly recapitulated changes in m⁶A, and we further showed that the loss of heterozygosity of *Mettl3* rescued m⁶A levels and the expression changes of some developmental genes in the fetal intestine that resulted from antibiotic treatment. Collectively, our data revealed that the maternal microbiome programs the m⁶A epitranscriptome of the mouse fetal brain and intestine.

Keywords: maternal microbiome, m⁶A, fetal development, Wnt signaling pathway, METTL3

INTRODUCTION

It is universally recognized that the microbiome exerts profound effects on host physiology and health, including host metabolism, circadian rhythm, intestinal morphology, and the development of the nervous system (Zhang et al., 2020; Brooks et al., 2021; Seki et al., 2021; Willyard, 2021; Wu J. et al., 2021; Wu Q. et al., 2021). Emerging studies have revealed that loss of the maternal microbiome impairs axonogenesis (Vuong et al., 2020), and that maternal exposure to antibiotics contributes to gut dysbiosis, immune dysfunction, and the occurrence of inflammatory bowel disease (IBD) in offspring (Miyoshi et al., 2017). These findings indicated that loss of the maternal microbiome impairs the fetal development and neonatal health in early life. However, the mechanisms underlying the actions of the maternal microbiome on the fetus remain elusive.

N6-methyladenosine (m⁶A) has been shown to be the most abundant and a highly conserved modification on messenger RNAs (mRNAs) and lncRNAs in mammals (Dominissini et al., 2012; Zhao et al., 2017a; Liu et al., 2020; Shu et al., 2020; Deng et al., 2021). mRNA m⁶A possesses a consensus motif of RRACH (R denoting G or A, and H reflecting A, C, or U) and it is principally found at stop codons, 3' untranslated regions (3'UTRs), and long exons (Dominissini et al., 2012;

Roundtree et al., 2017). m⁶A is produced by the METTL3–METTL14 core methyltransferase complex (Liu et al., 2014; Liu X. et al., 2021), erased by demethylases FTO and ALKBH5 (Jia et al., 2011; Zheng et al., 2013; Roundtree et al., 2017), and recognized by readers such as the YTH family proteins (Dominissini et al., 2012; Wang X. et al., 2014; Alarcón et al., 2015). m⁶A regulates various physiological processes, such as RNA stability (Dominissini et al., 2012; Wang X. et al., 2014; Alarcón et al., 2015; Huang et al., 2018), splicing (Xiao et al., 2016; Ke et al., 2017), translation (Meyer et al., 2015; Wang et al., 2015; Zhou et al., 2015; Shi et al., 2017), and signaling pathways (Li H.-B. et al., 2017; Huang H. et al., 2019; Uddin et al., 2021). Also, it occupies important roles in stem cell self-renewal (Li et al., 2018; Liu J. et al., 2021), embryonic development (Batista et al., 2014; Wang Y. et al., 2014; Chen et al., 2015; Geula et al., 2015; Vu et al., 2017; Bertero et al., 2018), tissue development (Zheng et al., 2013; Li H.-B. et al., 2017; Yoon et al., 2017; Zhao et al., 2017b; Wang et al., 2018), tumorigenesis (Ma et al., 2016; Li Z et al., 2017; Su et al., 2018; Huang Y et al., 2019; Su et al., 2020; Chen et al., 2021), and the progression of other human diseases (Fischer et al., 2009; Church et al., 2010; Mathiyalagan et al., 2019). It has been shown that the microbiome affects the mRNA m⁶A modification on the host tissues, especially the brain, intestine, and liver (Wang et al., 2019; Jabs et al., 2020). However, it remains unclear whether the maternal microbiome affects m⁶A epitranscriptome of the fetal brain, intestine, and liver so as to impact fetal development.

Herein, we demonstrated that the expression of m⁶A writers and erasers in the brain and intestine of the mouse fetus is altered by the maternal microbiome. Using MeRIP-seq, we systematically investigated the transcriptome-wide m⁶A methylome profiles of the mouse fetal brain and intestine, and we discovered that the maternal microbiome programs the fetal m⁶A methylome, and that m⁶A-modified genes regulated by the maternal microbiome are enriched in fetal neuro/intestine developmental pathways, such as the Wnt signaling. More importantly, antibiotic treatment recapitulated m⁶A alterations in the mouse fetal intestine and brain, and loss of heterozygosity of *Mettl3* rescued this effect. Our findings collectively indicate that the maternal microbiome programs the m⁶A epitranscriptome of the mouse fetal brain and intestine, and this may provide a promising basis to explore the mechanisms by which the maternal microbiome influences fetal development and diseases.

MATERIALS AND METHODS

Fetal Tissues Collection From SPF and GF Mice

Specific pathogen-free (SPF) pregnant mice ($n = 3$) and germ-free (GF) pregnant mice ($n = 3$) purchased from GemPharmatech Co., Ltd. were dissected on embryonic day 18 (E18), and the fetal

tissues (brain, intestine, and liver) were collected and stored at -80°C for subsequent analyses.

PCR Amplification and qPCR Analysis of 16S rRNA Genes

A total of 40 mg mouse fecal pellets were suspended in 200 μl lysis buffer (5 mM EDTA, 0.2% SDS, 0.2M NaCl, and 0.1M Tris-HCl) supplemented with 4 μl of 20 mg/ml proteinase K. The mixtures were disrupted with a grinding rod and then incubated at 56°C for 6 h. After centrifugation, the supernatant was used for 16S rRNA gene amplification, and the PCR products were visualized on a 2% agarose gel stained with ethidium bromide under UV light. The supernatant from CONV and ABX mice was used for the 16S rRNA gene qPCR analysis. The 16S rRNA gene was detected using two sets of universal bacterial primers: 27F and 1492R; 8F and 1541R. The primers are listed in **Supplementary Table S1**.

Tissues Lysate Preparation and Western Blots

Frozen tissues were homogenized and lysed in RIPA buffer (50 mM Tris-HCl pH 7.5, 1% Nonidet P-40, 0.5% sodium deoxycholate, 0.05% SDS, 1 mM EDTA, and 150 mM NaCl) with freshly added phosphatase inhibitors and protease inhibitors, and then centrifuged for 20 min at $13,000 \times g$. The supernatant was aspirated and loaded for the Western immunoblotting analysis. The following antibodies are used: METTL3 (A8370, Abclonal, 1:1,000), METTL14 (HPA038002, Sigma-Aldrich, 1:1,000), FTO (27226-1-AP, Proteintech, 1:1,000), ALKBH5 (16837-1-AP, Proteintech, 1:1,000), and β -actin (66009-1-Ig, Proteintech, 1:5,000).

RNA Isolation and mRNA Purification

Fetal mouse tissues were homogenized in 1 ml of TRNzol Universal Reagent (TIANGEN) with glass beads using a LUKYM-I homogenizer, and total RNA was isolated following the manufacturer's protocol. mRNA was separated from total RNA using a Dynabeads mRNA purification kit (Thermo Fisher Scientific), with two rounds of purification.

LC-MS/MS Quantification of m⁶A mRNA Modification

LC-MS/MS was performed essentially as described previously (Li et al., 2020). In brief, purified mRNA was digested to nucleosides by nuclease P1 and CIAP, and then it was diluted to 10 ng/ μl using nuclease-free water. The samples were filtered and injected into an Agilent Poroshell 120 column coupled online to an AB SCIEX Triple Quad 5500 LC mass spectrometer (Applied Biosystems) in a positive electrospray ionization mode. Concentrations of m⁶A and A were determined based on standard curves of the nucleosides, and the m⁶A/A ratio was calculated.

RT-qPCR

Total RNA (5 µg) from fetal mouse tissues was reverse-transcribed using a GoScript Reverse Transcription System (Promega), and quantitative real-time PCR was executed using a 2 × RealStar Green Power Mixture (GenStar). The fluorescence intensity of the amplification process was monitored using a LightCycler96 system (Roche). The primers are listed in **Supplementary Table S2**.

Methylated RNA Immunoprecipitation Sequencing

MeRIP experiments were executed as previously reported (Xiao et al., 2019). In brief, approximately 90 µg of total RNA was fragmented into 100- to 300-nucleotide (nt)-long fragments by zinc acetate, followed by the addition of EDTA to terminate the reaction. Then, 5 µg of fragmented RNA was taken as the input control and the remainder was incubated with m⁶A antibodies (4 µg, Abcam, ab151230) in IP buffer (150 mM NaCl, 0.05% NP-40, and 10 mM Tris-HCl) containing RNase inhibitor (Promega), and the mixture was subsequently bound to wash Dynabeads protein G (Invitrogen). After stringent wash, the m⁶A-containing fragments were eluted by competition with 1 mg/ml N⁶-methyladenosine (Selleck Chemicals). Both the immunoprecipitated RNA fragments and the input RNA were ultimately extracted for library construction using a SMARTer Stranded Total RNA-Seq Kit v2 - Pico Input Mammalian (Takara) following the manufacturer's protocol. We then performed sequencing using an Illumina Nova platform.

MeRIP-Seq Data Processing and Mapping

Prior to mapping, all raw data were filtered to remove adapters, and low-quality reads using Trimmomatic (Bolger et al., 2014). Reads of all samples that mapped to rRNA FASTA sequences from UCSC gene annotation (mm10) using bowtie2 (Langmead and Salzberg, 2012) were discarded, and the remaining reads were aligned to the mouse reference genome (GRCm38) using HISAT2 (Pertea et al., 2016). Then mapped files were filtered to keep unique and high mapping quality reads for further analysis using Picard and SAMtools (Li et al., 2009).

m⁶A Peak Calling

m⁶A peaks were identified using MeTPeak. A custom transcriptome annotation file, assembled by StringTie (Pertea et al., 2016) using all sample reads, was created to include intronic and intergenic m⁶A peaks. All other parameters were set to the default settings. The annotatePeaks.pl script from the Homer software suite (Heinz et al., 2010) was used for m⁶A peak annotation.

Evaluation of the Similarity of m⁶A Between Samples

m⁶A peaks identified in all samples were merged, and featureCounts (Liao et al., 2014) was used to count the fragments that were mapped to the merged peaks. The normalized fragment counts of each peak in MeRIP-seq

(MFPKM) were calculated using (methylated fragment counts mapped to the peak × 10⁹)/(length of the peak × total counts of the mapped fragment), and the normalized fragment counts of each peak in input-seq (IFPKM) were calculated using (input fragment counts mapped to the peak × 10⁹)/(length of the peak × total counts of mapped fragments). The methylation level was then calculated for each peak by dividing the MFPKM by the IFPKM. The Pearson correlation coefficient of log₂-scaled m⁶A levels across all samples was calculated using corrplot to represent the similarity of each sample.

Determination of m⁶A Motif and Distribution Pattern

m⁶A peaks were used for motif search using the findMotifsGenome.pl script from the Homer software suite, using “-rna” and “-len 5” parameters. The R package Guitar (Cui et al., 2016) was used to analyze and plot the distribution of m⁶A on mRNA.

Identification of Differentially Methylated Regions

The regions in which the GF group mean m⁶A level was 1.5 fold higher than the SPF group mean m⁶A level were defined as GF group up regions. Also, the regions in which the GF group mean m⁶A level was 1.5 fold lower than the SPF group mean m⁶A level were defined as GF group down regions.

Gene Ontology Analysis of Differential m⁶A-Methylated Genes

Differentially methylated regions were assigned to mouse genes using the annotatePeaks.pl script from the Homer software suite. The gene list was used for pathways and GO term enrichment using the clusterProfiler (Wu T. et al., 2021).

MeRIP-qPCR

The input RNA and the immunoprecipitated RNA fragments from mouse fetal tissues were reverse-transcribed using a GoScript Reverse Transcription System (Promega), and then they were analyzed using real-time qPCR. The ratio of immunoprecipitated RNA to the input of each peak was calculated and normalized to GAPDH. The primers are listed in **Supplementary Table S3**.

Cell Culture and Cell Line Generation

Mouse embryonic stem cell line E14TG2a (mES cells) was cultured with the N2B27 base medium supplemented with 1 mM glutamine (Invitrogen), 1% nonessential amino acids (Invitrogen), 0.15 mM 1-thioglycerol (Sigma), 100 U/ml of penicillin-streptomycin (Invitrogen), 25 µg/ml of BSA (Sigma), 1 µM MEK inhibitor PD0325901 (Selleck Chemicals), 3 µM GSK3β inhibitor CHIR99021 (Selleck Chemicals), 2% KOSR (Thermo Fisher), and 1000 U/ml of ESGRO leukemia inhibitory factor LIF (Millipore) on plates coated with 0.2% gelatin.

***Mettl3*^{-/-} mES Cell Line Generation**

The *Mettl3*^{-/-} mES cell line was generated using CRISPR-Cas9 as described previously (Shalem et al., 2014) and the sgRNA sequences are shown in **Supplementary Table S4**. In brief, sgRNAs were designed on <http://crispr-era.stanford.edu/> and cloned into the pXPR_001 plasmid. Then, pXPR_001 plasmid was transfected into mES cells using Lipofectamine 3000 (Invitrogen, L3000015). After 12 h, 3 μg/ml of puromycin was added and resistant cells were plated for single colony isolation. Colonies with the desired mutation were identified by Sanger sequencing.

RNA Stability Assay

mES cells cultured in 12-well plates at 70–80% confluency were treated with actinomycin D (5 μg/ml final concentration, MCE, HY-17559) for 0, 2, 4, and 8 h before being collected for the extraction of total RNA. RNA was then reverse-transcribed using GoScript Reverse Transcriptase (Promega), and analyzed using real-time qPCR. Expression levels of RNA were calculated and normalized to *GAPDH* first, and then to the 0 h time point. The mRNA stability of genes was estimated by the half-life of mRNA and calculated using GraphPad Prism 5.0. The primers are listed in **Supplementary Table S3**.

Animals

All of the mice were group-housed in a temperature-controlled (22 ± 1 °C) room with a 12:12-h light:dark cycle, and they had free access to food and water. *Mettl3*^{lox/+} mice were generated by Cyagen by inserting loxP sites with the same direction on both sides of exons 2 and 3 of the *Mettl3* gene. Male *Mettl3*^{lox/+} mice were crossed with female *Mettl3*^{lox/+} mice to obtain *Mettl3*^{lox/lox} mice. Next, *Mettl3*^{lox/lox} mice were first crossed with DDX4-Cre mice to generate *Mettl3*^{lox/+}; DDX4-Cre mice, and the latter were then crossed with wild-type mice to generate *Mettl3*^{-/+} heterozygous mice. The genotype of each mouse was determined using the genomic DNA extracted from tail tissue.

Antibiotic Treatment of Mice

To mimic GF status, conventional mice (CONV) were treated with antibiotics (ABX), based on methods previously described (Vuong et al., 2020). In brief, 10- to 12-week-old female mice were provided with a mixture of four antibiotics (vancomycin 0.5 g/L, neomycin 1 g/L, ampicillin 1 g/L, and amphotericin-B 0.1 g/L) in their water for 1 week. Female mice were then paired with male mice and gestational day 0.5 was determined by observation of a copulatory plug. Pregnant mice (*n* = 3) were maintained on ABX in their drinking water until embryonic day 18 (E18), and then dissected to obtain fetal tissues (brain and intestine).

Statistical Analysis

We expressed our measurement data as mean ± SEM. *T* tests were used for comparisons between two groups. Significant differences were represented by asterisks as follows: **p* < 0.05, ***p* < 0.01, and ****p* < 0.001, and ns, not significant.

RESULTS

Loss of the Maternal Microbiome Alters the Expression of m⁶A Writers and Erasers in the Fetal Brain and Intestine

We initially collected fecal pellets from germ-free (GF, *n* = 3) and specific pathogen-free (SPF, *n* = 3) pregnant mice, and the absence of intestinal microbiota in the GF mice was confirmed by 16S rRNA gene amplification (**Supplementary Figure S1A**). We, then, examined the levels of m⁶A regulators in the mouse fetal brain, intestine, and liver, including writers (METTL3 and METTL14), erasers (FTO and ALKBH5), and readers (YTH-domain family proteins). Using RT-qPCR, we determined that mRNA levels of m⁶A writers and erasers are highly expressed in the fetal brain and intestine from GF pregnant mice (hereafter designated GFB and GFI, respectively) compared to the corresponding tissues from SPF pregnant mice (hereafter designated SPFB and SPFI, respectively). However, the differences in m⁶A reader expression levels are much less marked (**Figures 1A,B**). Nevertheless, the expression of these proteins is similar in the fetal livers of these two types of mice (**Supplementary Figure S1B**). A similar tendency in the alteration of protein expression is also uncovered using the Western blotting analysis (**Figures 1C,D**). Taken together, these results indicated that loss of the maternal microbiome alters the expression of m⁶A writers and erasers in the fetal brain and intestine.

m⁶A Modification Profiles in the Fetal Brain and Intestine

To further investigate whether the maternal microbiome participates in modulating the m⁶A epitranscriptome of offspring, we first detected total m⁶A levels of mouse fetal tissues. We did not observe an apparent change in the global mRNA m⁶A levels between SPF and GF mice as revealed by LC-MS/MS (**Supplementary Figure S2A**). We, thus, characterized m⁶A methylomes of both mouse fetal brain and intestine (SPFB and GFB and SPFI and GFI—using two independent biological replicates for both) by an m⁶A-immunoprecipitation sequencing (MeRIP-seq) analysis. The samples of the same tissue type were clustered well (**Figure 2A**) and the classic GGAC motif was observed in the fetal brain and intestine (**Figure 2B**). In agreement with previous studies (Dominissini et al., 2012; Roundtree et al., 2017), the distribution of m⁶A signals around mRNA in the two types of fetal tissue samples was mostly presented in the CDS and 3'UTR, and to a lesser extent in the 5'UTR (**Figure 2C**). We identified the numbers of m⁶A peaks from these fetal tissues (17,526 in SPFB, 16,885 in GFB, 14,436 in SPFI, and 13,781 in GFI), and we ascertained that approximately three-fourths of the m⁶A peaks overlapped in both fetal brain and intestine (**Figure 2D**). Compared with SPFB, GFB showed some changes in patterns of m⁶A peaks, with a relative elevation in exonic (SPF 26.81% vs. GFB 28%) and intronic regions (SPF 27.86% vs. GFB 29.38%), and a relative diminution in the 3'untranslated region

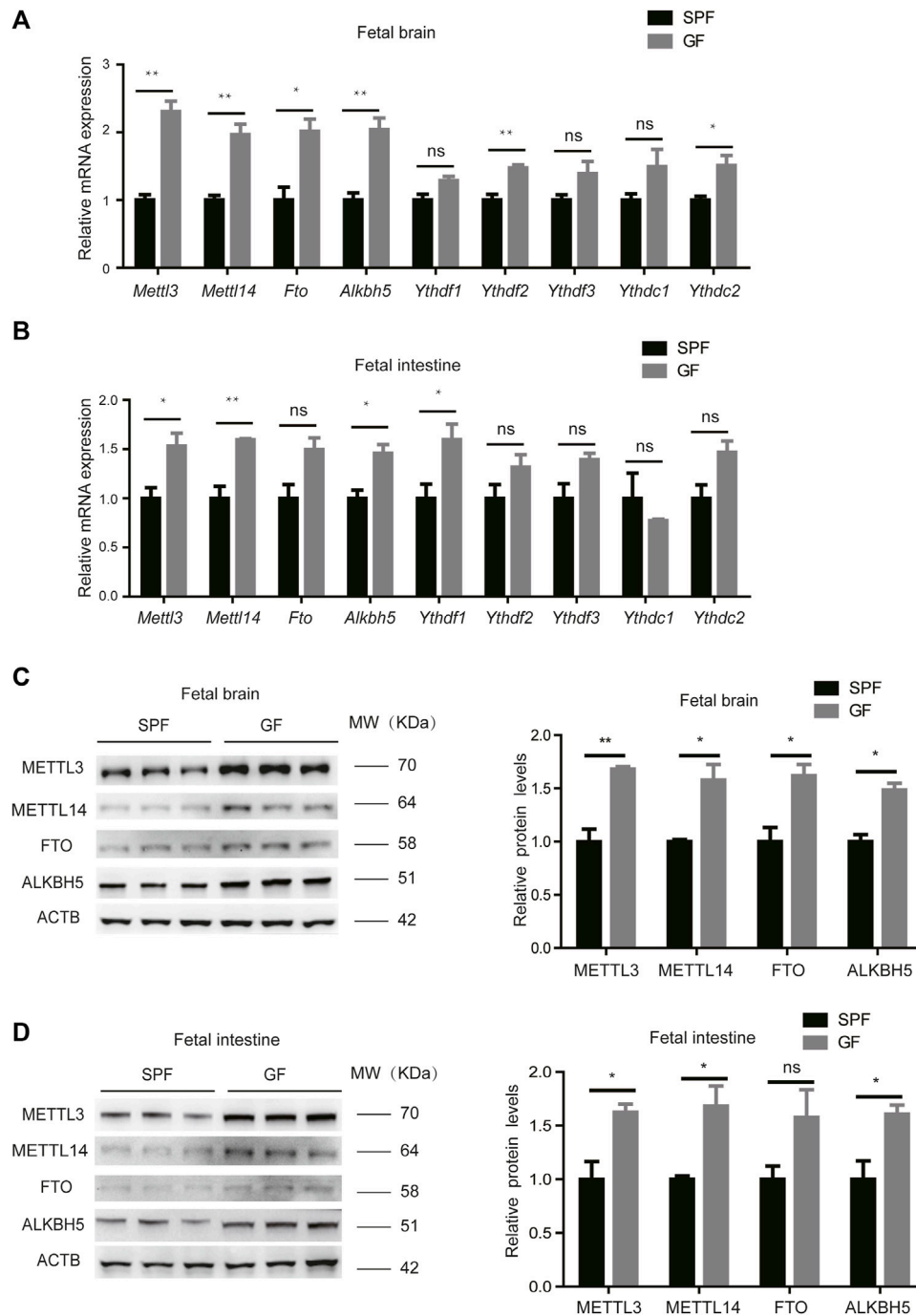


FIGURE 1 | Loss of the maternal microbiome alters the expression of m⁶A writers and erasers in fetal mice. **(A,B)** Relative mRNA expression levels of m⁶A writers, erasers, and readers in fetal brains **(A)** and intestines **(B)** of SPF and GF mice. **(C,D)** Western blots showing the protein expression of m⁶A writers and erasers in fetal brains **(C)** and intestines **(D)** of SPF and GF mice, and relative protein expression levels were calculated based on the band density in Western blotting results.

(3'UTR) from 18 to 16.96% (**Figure 2E**). Compared with SPFI, the GFI also showed some alterations in patterns of m⁶A peaks with a relative augmentation in exonic regions (SPFI 30.68% vs. GFI 32.5%), and a relative reduction in intronic regions from 30.12 to 29.18% and intergenic regions of 7.7–6.41% (**Figure 2F**).

The Maternal Microbiome Regulates the m⁶A of Neurodevelopment Genes in the Mouse Fetal Brain

To investigate the dynamic characteristics of m⁶A methylation, we further analyzed the differential m⁶A peaks in mouse fetal

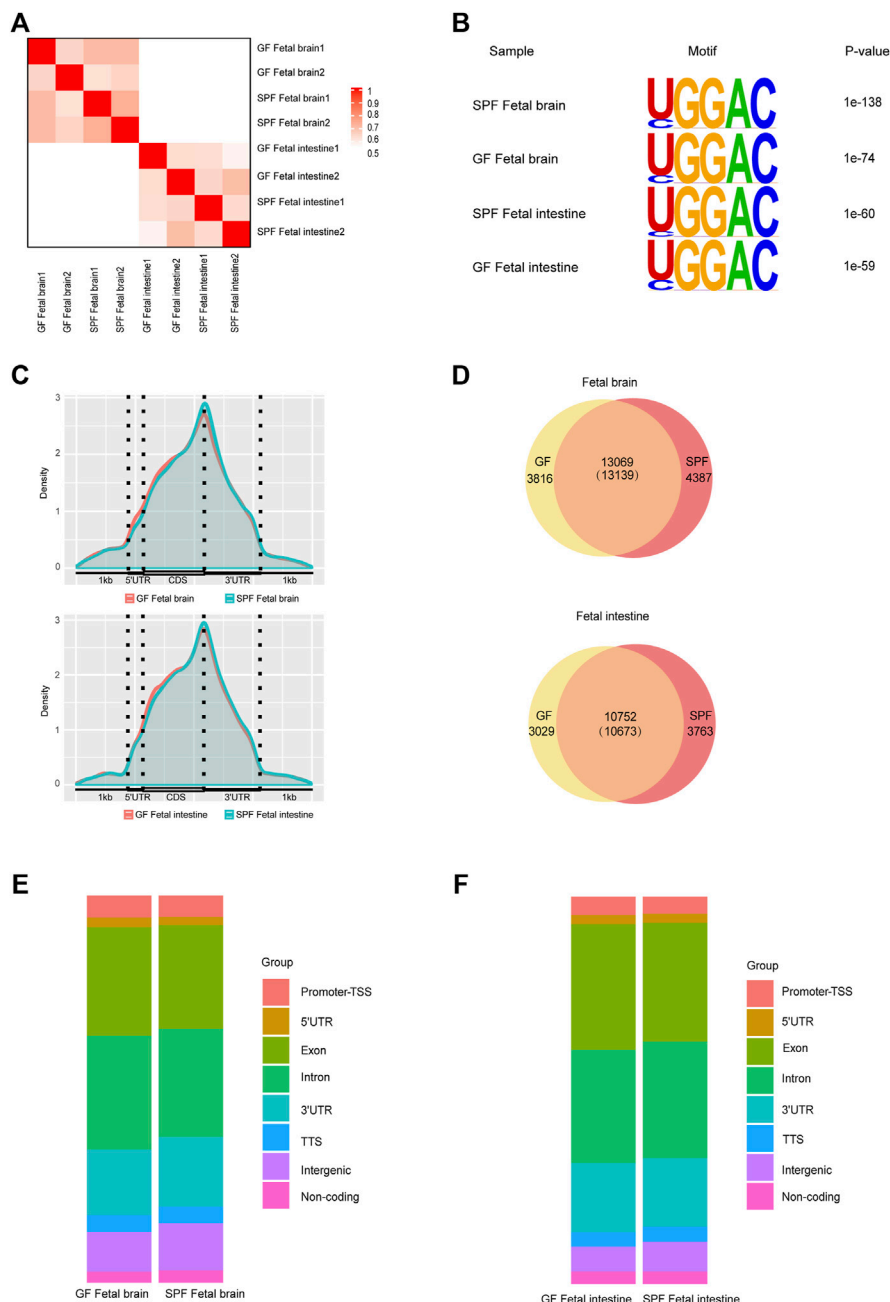
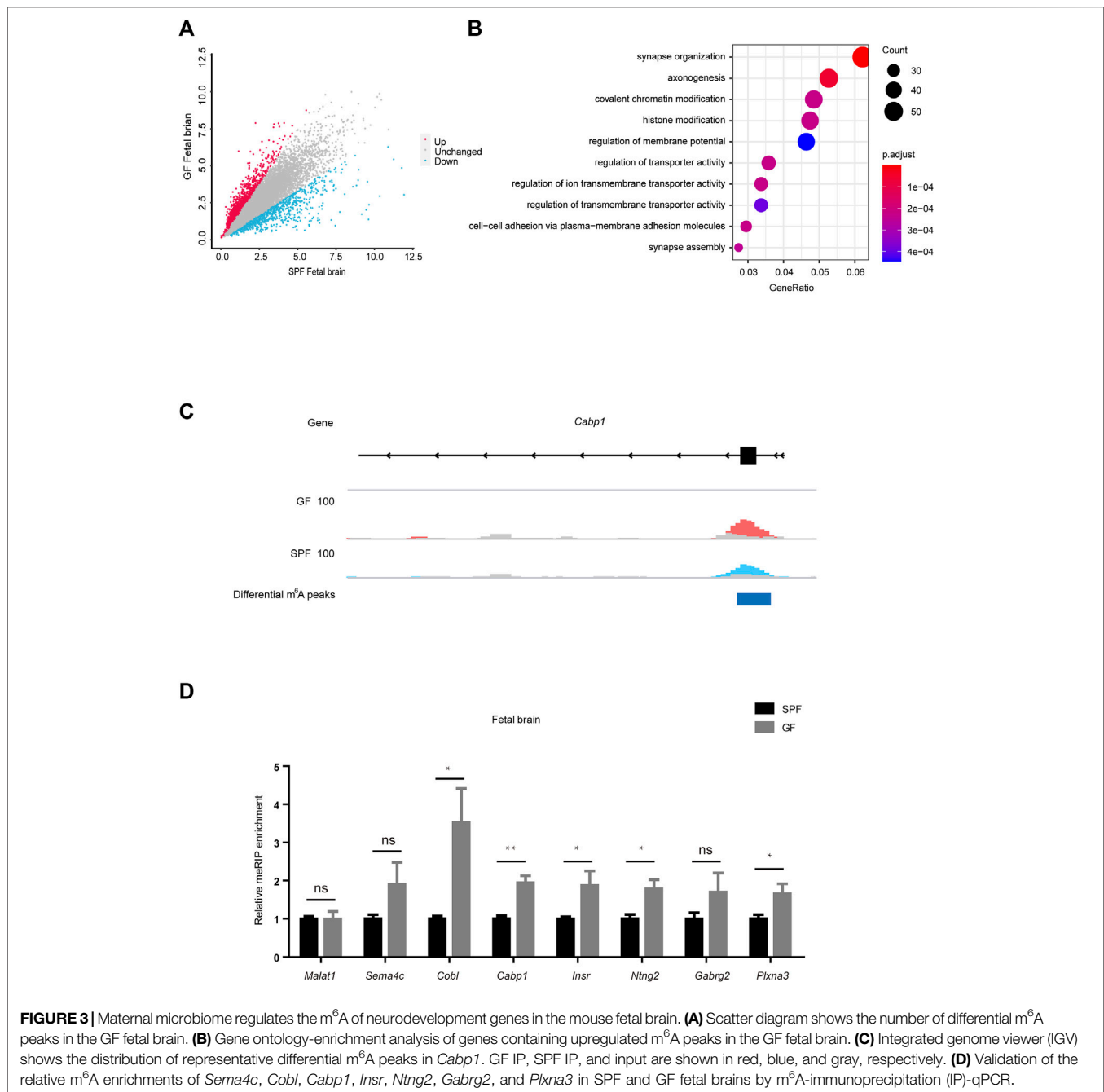


FIGURE 2 | Modification profiles of m⁶A in the fetal brain and intestine. **(A)** Similarity (using Pearson's correlation) of m⁶A peaks between each pair of samples. **(B)** Motif analysis of m⁶A peaks in fetal brains and intestines of SPF and GF mice. **(C)** Pattern distribution of m⁶A across the mRNA regions in the fetal brain and intestine. m⁶A peaks were mapped back to the corresponding genes, and assigned as originating from the 5'-UTR, coding sequence (CDS), or 3'-UTR. **(D)** Venn diagram showing the overlap of m⁶A peaks between fetal brains and intestines of SPF and GF mice. **(E,F)** Bar charts showing the distribution of m⁶A peaks in the fetal brain **(E)** and intestine **(F)**.

tissues. As shown in **Figure 3A**, GFB manifested 2072 upregulated m⁶A peaks and 583 downregulated m⁶A peaks (with the criterion of fold-change ≥ 1.5). In further examination of the genomic distribution in all three mRNA regions of differential m⁶A peaks, we demonstrated that a majority of the differential m⁶A peaks were in CDS and 3'UTR (**Supplementary Figure S3A**). Mapping these reads of

differential m⁶A peaks to the genome, we identified 1147 genes with upregulated m⁶A peaks and 496 genes with downregulated m⁶A peaks (**Supplementary Figure S3B**). To further study the biological significance of dysregulated m⁶A modifications in the fetal brain, we conducted GO analyses of differentially m⁶A-methylated genes (**Figure 3B** and **Supplementary Figure S3C**). We concentrated on the function of m⁶A-hypermethylated



genes and showed that these genes were significantly enriched in pathways related to neurodevelopment, such as synapse formation and axonogenesis. The read coverage plot of a representative gene *Cabp1* associated with neurodevelopment was depicted in **Figure 3C**, and the m⁶A levels of genes (*Sema4c*, *Cobl*, *Cabp1*, *Insr*, *Ntng2*, *Gabrg2*, and *Plxna3*) were increased in GFB as revealed by using the MeRIP-qPCR analysis (**Figure 3D**). In addition, the transcript levels of these genes were confirmed by using the RT-qPCR analysis (**Supplementary Figure S3D**). Collectively, these data suggest that the maternal

microbiome regulates the m⁶A of neurodevelopment genes in the mouse fetal brain.

The Maternal Microbiome Regulates Fetal Intestinal m⁶A-Modified Genes in the Wnt Signaling Pathway

As shown in **Figure 4A**, GFI reflected 2068 upregulated m⁶A peaks and 184 downregulated m⁶A peaks (with a fold-change ≥ 1.5). Further examination of the genomic distribution in all three mRNA regions of

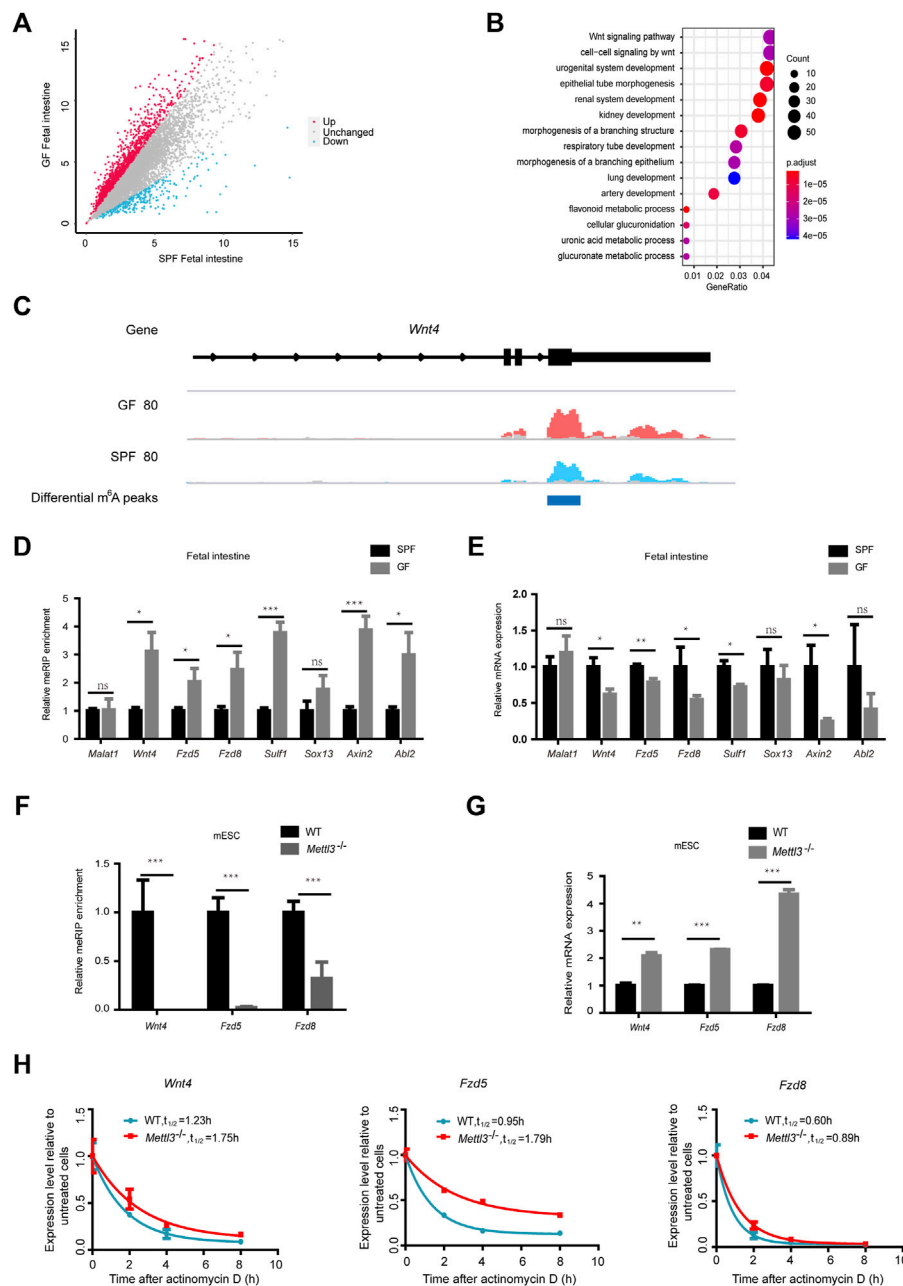


FIGURE 4 | Maternal microbiome regulates fetal intestinal m⁶A-modified genes in the Wnt signaling pathway. **(A)** Scatter diagram shows the number of differential m⁶A peaks in the GF fetal intestine. **(B)** Gene ontology-enrichment analysis of genes containing upregulated m⁶A peaks in the GF fetal intestine. **(C)** IGV shows the distribution of representative differential m⁶A peaks in *Wnt4*. GF IP, SPF IP, and input are shown in red, blue, and gray, respectively. **(D)** Validation of the relative m⁶A enrichments of *Wnt4*, *Fzd5*, *Fzd8*, *Sulf1*, *Sox13*, *Axin2*, and *Abi2* in SPF and GF fetal intestines by m⁶A-immunoprecipitation (IP)-qPCR. **(E)** Validation of the relative mRNA expression levels of *Wnt4*, *Fzd5*, *Fzd8*, *Sulf1*, *Sox13*, *Axin2*, and *Abi2* in SPF and GF fetal intestines. **(F)** Validation of the relative m⁶A enrichments of *Wnt4*, *Fzd5*, and *Fzd8* in the WT and *Mettl3*^{-/-} mouse embryonic stem cell line E14TG2a by m⁶A-immunoprecipitation (IP)-qPCR. **(G)** Validation of the relative mRNA expression levels of *Wnt4*, *Fzd5*, and *Fzd8* in the WT and *Mettl3*^{-/-} mouse embryonic stem cell line E14TG2a. **(H)** Half-life ($t_{1/2}$) of *Wnt4*, *Fzd5*, and *Fzd8* mRNA in the WT and *Mettl3*^{-/-} mouse embryonic stem cell line E14TG2a after actinomycin D treatment.

the differential m⁶A peaks revealed that most of the differential m⁶A peaks were in CDS and 3'UTR (**Supplementary Figure S4A**). When we mapped these reads of differential m⁶A peaks to the genome, we identified 1590 genes with upregulated m⁶A peaks and 166 genes with downregulated m⁶A peaks (**Supplementary Figure S4B**). To further

assess the biological significance of dysregulated m⁶A modification in the fetal intestine, we executed GO analysis of differentially m⁶A-methylated genes (**Figure 4B** and **Supplementary Figure S4C**). When we concentrated on the functions of m⁶A-hypermethylated genes, we found that they were significantly

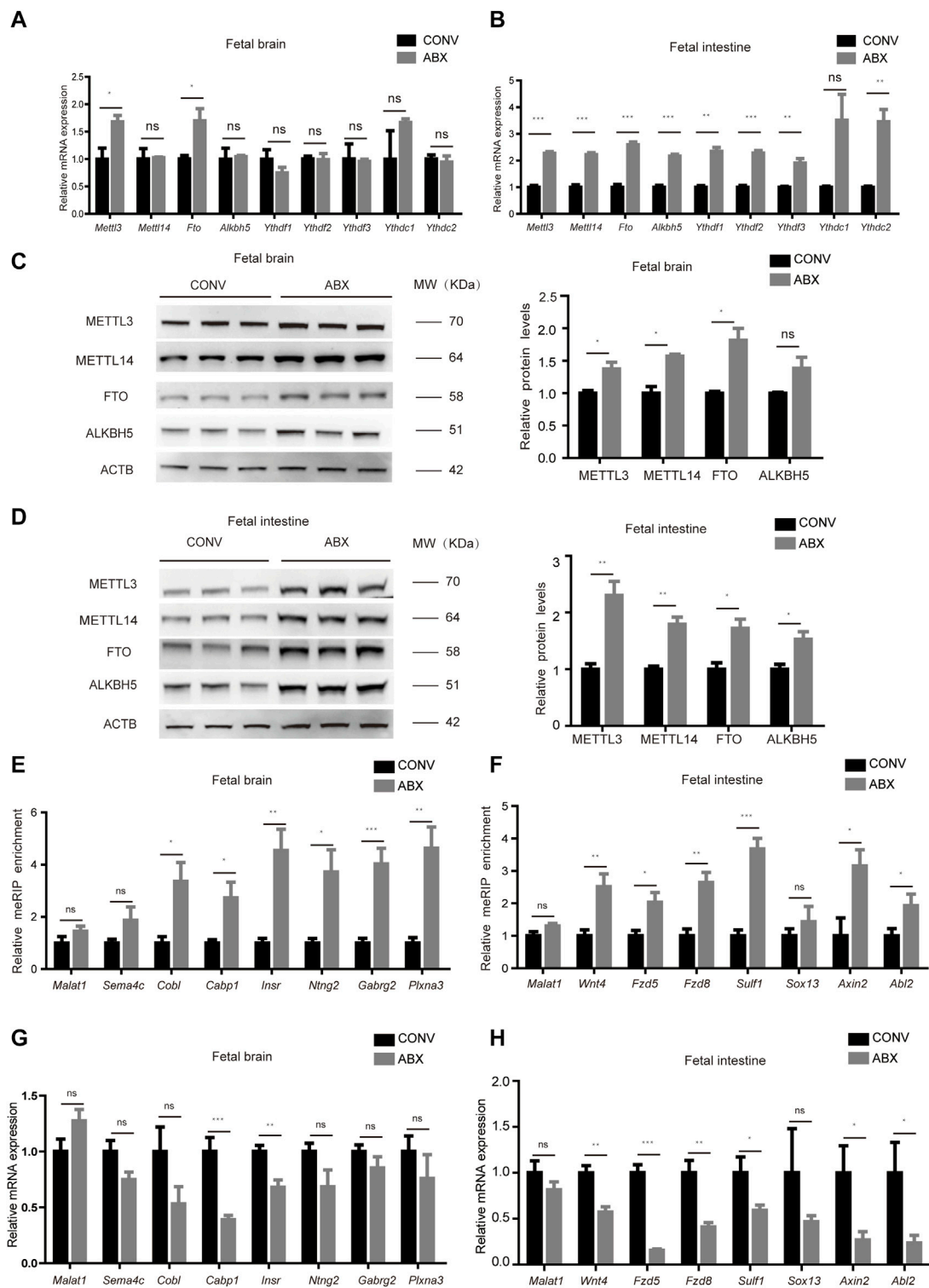


FIGURE 5 | Antibiotic treatment mostly recapitulates m⁶A alterations in the mouse fetal intestine and brain. **(A,B)** Relative mRNA expression levels of m⁶A writers and erasers in CONV and ABX fetal brains **(A)** and intestines **(B)**. **(C,D)** Western blot shows the protein expression levels of m⁶A writers and erasers in fetal brains **(C)** and intestines **(D)** of CONV and ABX mice, and relative protein expression levels were calculated based on the band density in Western blotting results. **(E,G)** Validation of the relative m⁶A enrichment of *Sema4c*, *Cobl*, *Cabp1*, *Insr*, *Ntng2*, *Gabrg2*, and *Plxna3* in CONV and ABX fetal brains **(E)** and of *Wnt4*, *Fzd5*, *Fzd8*, *Sulf1*, *Sox13*, *Axin2*, and *Abl2* in CONV and ABX fetal intestines **(G)** by m⁶A-immunoprecipitation (IP)-qPCR. **(F,H)** Validation of the relative mRNA expression levels of *Sema4c*, *Cobl*, *Cabp1*, *Insr*, *Ntng2*, *Gabrg2*, and *Plxna3* in CONV and ABX fetal brains **(F)** and of *Wnt4*, *Fzd5*, *Fzd8*, *Sulf1*, *Sox13*, *Axin2*, and *Abl2* in CONV and ABX fetal intestines **(H)**.

enriched in the Wnt signaling pathway. The read coverage plot of a representative gene *Wnt4* is shown in **Figure 4C**. The differential m⁶A levels of representative genes (*Wnt4*, *Fzd5*, *Fzd8*, *Sulf1*, *Sox13*, *Axin2*, and *Abl2*) were confirmed by the MeRIP-qPCR analysis (**Figure 4D**), and their transcript levels were all attenuated in GFI compared to SPFI as revealed by the RT-qPCR analysis (**Figure 4E**). This indicates that differential m⁶A modifications in these two types of fetal intestines are correlated with the expression of genes enriched in the Wnt signaling pathways. Next, we knocked out *Mettl3* (*Mettl3*^{-/-}) in the mES cell line using CRISPR/Cas9, and we consistently found that *Mettl3* knockout significantly decreased m⁶A levels of representative genes while increasing mRNA expression levels (**Figures 4F,G**). We further investigated whether the changes in m⁶A methylation would affect mRNA levels of representative genes in mESC. We observed that in the presence of actinomycin D (an inhibitor of mRNA transcription), *Mettl3* knockout retards the degradation of representative genes mRNAs (**Figure 4H**). Collectively, these data suggest that the maternal microbiome regulates fetal intestinal m⁶A-modified genes in the Wnt signaling pathway.

Antibiotic Treatment Mostly Recapitulates m⁶A Change in the Mouse Fetal Intestine and Brain

To confirm the aforementioned results, we treated CONV pregnant mice with a mixture of four antibiotics (vancomycin, neomycin, ampicillin, and amphotericin-B) to mimic germ-free status (ABX mice) and validated that intestinal microbiota were almost exhausted by the 16S rRNA gene qPCR analysis (**Supplementary Figure S5A**). Similar to our previous experimental results, the mRNA expression levels of *Mettl3* and *Fto* in the ABX fetal brain were slightly higher than those in the CONV fetal brain (**Figure 5A**), while the mRNA expression levels of both m⁶A writers and erasers in the ABX fetal intestine were significantly increased compared to the CONV fetal intestine (**Figure 5B**). In addition, the expression of these proteins remained unchanged in fetal livers from both CONV and ABX (**Supplementary Figure S5B**). As for the protein expression levels of m⁶A writers and erasers, we noted a universal tendency for them to increase in the ABX fetal brain and intestine (**Figures 5C,D**). We then determined the m⁶A levels and the expression of representative genes regulated by the maternal microbiome in the ABX and CONV fetal brain and intestine, and we found that the m⁶A levels of these genes in the ABX brain and intestine were also increased relative to CONV (**Figures 5E,F**), and their transcript levels were confirmed by the RT-qPCR analysis (**Figures 5G,H**). Collectively, these data show that antibiotic treatment mostly recapitulates m⁶A alterations in the mouse fetal intestine and brain.

Loss of Heterozygosity of *Mettl3* Inhibits the Susceptibility of the Mouse Fetal Intestine to the Maternal Microbiome

To further confirm that the expression of developmental genes was regulated by m⁶A as programed by the maternal microbiome, we

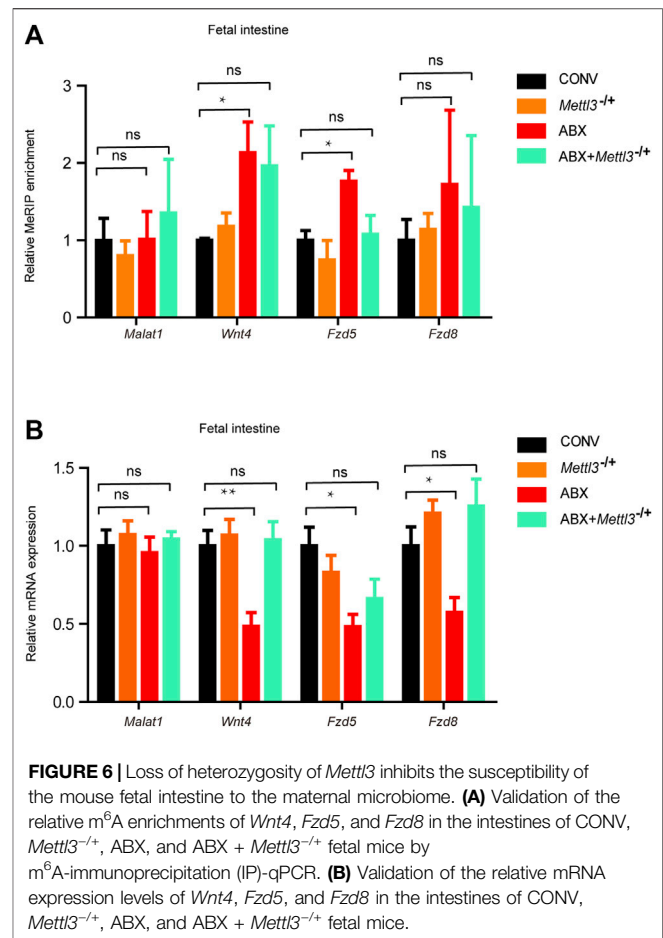


FIGURE 6 | Loss of heterozygosity of *Mettl3* inhibits the susceptibility of the mouse fetal intestine to the maternal microbiome. **(A)** Validation of the relative m⁶A enrichments of *Wnt4*, *Fzd5*, and *Fzd8* in the intestines of CONV, *Mettl3*^{-/-}, ABX, and ABX + *Mettl3*^{-/-} fetal mice by m⁶A-immunoprecipitation (IP)-qPCR. **(B)** Validation of the relative mRNA expression levels of *Wnt4*, *Fzd5*, and *Fzd8* in the intestines of CONV, *Mettl3*^{-/-}, ABX, and ABX + *Mettl3*^{-/-} fetal mice.

generated *Mettl3*^{-/-} heterozygous mice (**Supplementary Figures S6A,B**). Because the homozygous knockout of *Mettl3* was embryonically lethal, we crossed *Mettl3* heterozygous knockout male mice (*Mettl3*^{-/-}) with wild-type (WT) female mice. The latter were provided with water (i.e., the offspring of CONV and *Mettl3*^{-/-} mice) or ABX (i.e., the offspring of ABX and *Mettl3*^{-/-} mice). As expected, there were no significant differences in m⁶A levels of representative genes between CONV and *Mettl3*^{-/-} fetal intestines, however, m⁶A levels of representative genes increased in the ABX fetal intestine but not in the ABX + *Mettl3*^{-/-} fetal intestine, compared with the CONV fetal intestine (**Figure 6A**). Correspondingly, mRNA expression levels of representative genes showed no differences between CONV and *Mettl3*^{-/-} fetal intestines, while they were significantly reduced in the ABX fetal intestine but not in the ABX + *Mettl3*^{-/-} fetal intestine, compared with the CONV fetal intestine (**Figure 6B**). Our collective results, therefore, indicate that the maternal microbiome affects the developmental gene expression via m⁶A modifications.

DISCUSSION

The microbiome and m⁶A modifications are closely related to human health and disease, and previous studies have shown that host m⁶A is strongly affected by the mouse microbiome (Wang et al., 2019; Jabs

et al., 2020). However, the impact of the maternal microbiome on the m⁶A epitranscriptome of the mouse fetus has not yet been elucidated. In this study, we profiled the transcriptome-wide m⁶A methylome of the mouse fetal brain and intestine, demonstrated the alterations in m⁶A methylation caused by the maternal microbiome, identified differential m⁶A peaks, and showed that genes with dysregulated m⁶A peaks were potentially active in fetal development.

In a recent study, Wang et al. (2019) ascertained that both m⁶A writers and erasers were highly overexpressed in the GF brain compared to the SPF brain regardless of RNA and protein levels. Intriguingly, our results also revealed that the maternal microbiome also altered the expression of m⁶A writers and erasers in the mouse fetal brain and intestine, and that expression was recapitulated by antibiotic treatment.

Previous studies have depicted depletion of the maternal microbiome as impairing fetal thalamocortical axonogenesis (Vuong et al., 2020). Our results suggested that loss of the maternal microbiome contributed to m⁶A-hypermethylated genes in GFB, and that these genes were significantly enriched in pathways related to neurodevelopment, including synapse formation and axonogenesis. Moreover, the mRNA expression levels of these m⁶A-hypermethylated genes were commensurately altered, implying that m⁶A plays a key role in effects engendered by the maternal microbiome on fetal neurodevelopment. It is worth noting that increasing evidence reveals a functional link between gut bacteria and neurodegenerative diseases such as Alzheimer's disease and Parkinson's diseases (Sampson et al., 2016; Bhattarai et al., 2021; Willyard, 2021), and the abnormality in m⁶A is involved in neurological dysfunction and behavioral defects (Mitropoulos et al., 2017; Chen et al., 2019; Han et al., 2020; Huang et al., 2020). However, although it remains elusive whether the regulation of fetal neurodevelopment by the maternal gestational microbiome increases the risk of neurologic diseases in adulthood, we expect that the elucidation of such a mechanism will provide a foundation for future novel treatments of nerve diseases.

The Wnt signaling pathway is highly conserved from nematodes to mammals (Kohn and Moon, 2005; Clevers and Nusse, 2012) and is involved in many aspects of embryonic development (Clevers, 2006; MacDonald et al., 2009). Current evidence indicates that the Wnt signaling pathway regulates the self-renewal or differentiation of intestinal stem cells (Reya and Clevers, 2005; Böttcher et al., 2021). Our results showed that upregulated m⁶A genes in GFI were enriched in the Wnt signaling pathway but that mRNA expression levels of these genes were downregulated compared with SPFI, the mechanism of which is that m⁶A accelerates the degradation of these genes mRNA. These results reveal that the maternal microbiome regulates the gene expression in Wnt signaling by m⁶A in the fetal intestine, and this may constitute a mechanism whereby loss of the maternal microbiome

impairs fetal intestinal development. In addition, maternal exposure to antibiotics promotes gut dysbiosis and increases the risk of inflammatory bowel diseases in offspring (Miyoshi et al., 2017). Although such data suggest that the maternal gestational microbiome exerts a critical effect on the onset and progression of intestinal diseases in offspring, the precise role of m⁶A in this action requires further clarification.

For further verification, we treated conventional mice (CONV) with antibiotics (ABX) to mimic GF status. Although antibiotic treatment mostly recapitulates m⁶A change in mouse fetus, some differences in m⁶A epitranscriptome between GF and ABX mouse still exist. For example, the mRNA expression levels of *Mettl14* and *Alkbh5* were increased in GFB but not in the ABX mouse fetal brain, which may be caused by some individual differences among different mice due to age, nutritional status, or other factors (Jabs et al., 2020). In addition, ABX treatments are unable to completely eradicate the microbiome so there still exists a small amount (about 5%) of the microbiome in ABX mice compared with GF mice, and the acute or subacute aseptic state simulated by antibiotic treatment is not exactly the same as the chronic rearing under an aseptic environment for a long time (Vuong et al., 2020), which may also be some important reasons why the m⁶A epitranscriptome of GF mouse has some difference from the ABX mouse.

Collectively, our data reveal programing of the maternal microbiome on m⁶A modifications in the mouse fetus and should assist in unveiling the underlying mechanisms by which gut dysbiosis precipitates human disease. With progressively maturing analyses and technical developments, we expect that m⁶A will evolve into a potential therapeutic target of microbiota-directed disease.

DATA AVAILABILITY STATEMENT

The datasets presented in this study can be found in online repositories. The names of the repository and accession number can be found as follows: <http://bigd.big.ac.cn/gsa>, CRA006146.

ETHICS STATEMENT

The animal study was reviewed and approved by the Southern Medical University Experimental Animal Ethics Committee. Guangzhou, China.

AUTHOR CONTRIBUTIONS

YL, ZhW, and LX designed and supervised the project. ZX, SL, ZL, JC, HW, ZiW, and QR performed experiments. ZL and JC

conducted the bioinformatic analysis. YL and ZX wrote the manuscript with input from all authors.

FUNDING

This work was supported by the National Key R&D Program of China (grant nos. 2019YFA0802303 and 2021YFA0805400), the Guangdong Basic and Applied Basic Research Foundation (grant no. 2022A1515011821), and the National Demonstration Center for Experimental Education of Basic Medical Sciences (Southern Medical University).

REFERENCES

- Alarcón, C. R., Goodarzi, H., Lee, H., Liu, X., Tavazoie, S., and Tavazoie, S. F. (2015). HNRNPA2B1 Is a Mediator of m⁶A-dependent Nuclear RNA Processing Events. *Cell* 162 (6), 1299–1308. doi:10.1016/j.cell.2015.08.011
- Batista, P. J., Molinie, B., Wang, J., Qu, K., Zhang, J., Li, L., et al. (2014). m⁶A RNA Modification Controls Cell Fate Transition in Mammalian Embryonic Stem Cells. *Cell Stem Cell* 15 (6), 707–719. doi:10.1016/j.stem.2014.09.019
- Bertero, A., Brown, S., Madrigal, P., Osnato, A., Ortmann, D., Yiangou, L., et al. (2018). The SMAD2/3 Interactome Reveals that TGFβ Controls m⁶A mRNA Methylation in Pluripotency. *Nature* 555 (7695), 256–259. doi:10.1038/nature25784
- Bhattarai, Y., Si, J., Pu, M., Ross, O. A., McLean, P. J., Till, L., et al. (2021). Role of Gut Microbiota in Regulating Gastrointestinal Dysfunction and Motor Symptoms in a Mouse Model of Parkinson's Disease. *Gut Microbes* 13 (1), 1866974. doi:10.1080/19490976.2020.1866974
- Bolger, A. M., Lohse, M., and Usadel, B. (2014). Trimmomatic: A Flexible Trimmer for Illumina Sequence Data. *Bioinformatics* 30 (15), 2114–2120. doi:10.1093/bioinformatics/btu170
- Böttcher, A., Büttner, M., Tritschler, S., Sterr, M., Aliluev, A., Oppenländer, L., et al. (2021). Non-canonical Wnt/PCP Signalling Regulates Intestinal Stem Cell Lineage Priming towards Enteroendocrine and Paneth Cell Fates. *Nat. Cell Biol.* 23 (1), 23–31. doi:10.1038/s41556-020-00617-2
- Brooks, J. F., Behrendt, C. L., Ruhn, K. A., Lee, S., Raj, P., Takahashi, J. S., et al. (2021). The Microbiota Coordinates Diurnal Rhythms in Innate Immunity with the Circadian Clock. *Cell* 184 (16), 4154–4167. doi:10.1016/j.cell.2021.07.001
- Chen, H., Gao, S., Liu, W., Wong, C.-C., Wu, J., Wu, J., et al. (2021). RNA N⁶-Methyladenosine Methyltransferase METTL3 Facilitates Colorectal Cancer by Activating the m⁶A-GLUT1-mTORC1 axis and Is a Therapeutic Target. *Gastroenterology* 160 (4), 1284–1300. doi:10.1053/j.gastro.2020.11.013
- Chen, T., Hao, Y.-J., Zhang, Y., Li, M.-M., Wang, M., Han, W., et al. (2015). m⁶A RNA Methylation Is Regulated by MicroRNAs and Promotes Reprogramming to Pluripotency. *Cell Stem Cell* 16 (3), 289–301. doi:10.1016/j.stem.2015.01.016
- Chen, X., Yu, C., Guo, M., Zheng, X., Ali, S., Huang, H., et al. (2019). Down-Regulation of m⁶A mRNA Methylation Is Involved in Dopaminergic Neuronal Death. *ACS Chem. Neurosci.* 10 (5), 2355–2363. doi:10.1021/acchemneuro.8b00657
- Church, C., Moir, L., McMurray, F., Girard, C., Banks, G. T., Teboul, L., et al. (2010). Overexpression of Fto Leads to Increased Food Intake and Results in Obesity. *Nat. Genet.* 42 (12), 1086–1092. doi:10.1038/ng.713
- Clevers, H., and Nusse, R. (2012). Wnt/β-Catenin Signaling and Disease. *Cell* 149 (6), 1192–1205. doi:10.1016/j.cell.2012.05.012
- Clevers, H. (2006). Wnt/β-Catenin Signaling in Development and Disease. *Cell* 127 (3), 469–480. doi:10.1016/j.cell.2006.10.018
- Cui, X., Wei, Z., Zhang, L., Liu, H., Sun, L., Zhang, S.-W., et al. (2016). Guitar: An R/Bioconductor Package for Gene Annotation Guided Transcriptomic Analysis of RNA-Related Genomic Features. *BioMed Res. Int.* 2016, 1–8. doi:10.1155/2016/8367534
- Deng, S., Zhang, H., Zhu, K., Li, X., Ye, Y., Li, R., et al. (2021). M6A2Target: A Comprehensive Database for Targets of m⁶A Writers, Erasers and Readers. *Brief. Bioinform.* 22 (3), bbaa055. doi:10.1093/bib/bbaa055

ACKNOWLEDGMENTS

We thank S. Xiao for discussion and critical reading of the manuscript.

SUPPLEMENTARY MATERIAL

The Supplementary Material for this article can be found online at: <https://www.frontiersin.org/articles/10.3389/fcell.2022.882994/full#supplementary-material>

- Dominissini, D., Moshitch-Moshkovitz, S., Schwartz, S., Salmon-Divon, M., Ungar, L., Osenberg, S., et al. (2012). Topology of the Human and Mouse m⁶A RNA Methylomes Revealed by m⁶A-Seq. *Nature* 485 (7397), 201–206. doi:10.1038/nature11112
- Fischer, J., Koch, L., Emmerling, C., Vierkotten, J., Peters, T., Brüning, J. C., et al. (2009). Inactivation of the Fto Gene Protects from Obesity. *Nature* 458 (7240), 894–898. doi:10.1038/nature07848
- Geula, S., Moshitch-Moshkovitz, S., Dominissini, D., Mansour, A. A., Kol, N., Salmon-Divon, M., et al. (2015). m⁶A mRNA Methylation Facilitates Resolution of Naïve Pluripotency toward Differentiation. *Science* 347 (6225), 1002–1006. doi:10.1126/science.1261417
- Han, M., Liu, Z., Xu, Y., Liu, X., Wang, D., Li, F., et al. (2020). Abnormality of m⁶A mRNA Methylation Is Involved in Alzheimer's Disease. *Front. Neurosci.* 14, 98. doi:10.3389/fnins.2020.00098
- Heinz, S., Benner, C., Spann, N., Bertolino, E., Lin, Y. C., Laslo, P., et al. (2010). Simple Combinations of Lineage-Determining Transcription Factors Prime Cis-Regulatory Elements Required for Macrophage and B Cell Identities. *Mol. Cell* 38 (4), 576–589. doi:10.1016/j.molcel.2010.05.004
- Huang, H., Camats-Perna, J., Medeiros, R., Anggono, V., and Widagdo, J. (2020). Altered Expression of the m⁶A Methyltransferase METTL3 in Alzheimer's Disease. *eNeuro* 7 (5), 0125. doi:10.1523/ENEURO.0125-20.2020
- Huang, H., Weng, H., Sun, W., Qin, X., Shi, H., Wu, H., et al. (2018). Recognition of RNA N⁶-Methyladenosine by IGF2BP Proteins Enhances mRNA Stability and Translation. *Nat. Cell Biol.* 20 (3), 285–295. doi:10.1038/s41556-018-0045-z
- Huang, H., Weng, H., Zhou, K., Wu, T., Zhao, B. S., Sun, M., et al. (2019). Histone H3 Trimethylation at Lysine 36 Guides m⁶A RNA Modification Co-transcriptionally. *Nature* 567 (7748), 414–419. doi:10.1038/s41586-019-1016-7
- Huang, Y., Su, R., Sheng, Y., Dong, L., Dong, Z., Xu, H., et al. (2019). Small-Molecule Targeting of Oncogenic FTO Demethylase in Acute Myeloid Leukemia. *Cancer Cell* 35 (4), 677–691. doi:10.1016/j.ccell.2019.03.006
- Jabs, S., Biton, A., Bécavin, C., Nahori, M.-A., Ghazlane, A., Pagliuso, A., et al. (2020). Impact of the Gut Microbiota on the m⁶A Epitranscriptome of Mouse Cecum and Liver. *Nat. Commun.* 11 (1), 1344. doi:10.1038/s41467-020-15126-x
- Jia, G., Fu, Y., Zhao, X., Dai, Q., Zheng, G., Yang, Y., et al. (2011). N⁶-Methyladenosine in Nuclear RNA Is a Major Substrate of the Obesity-Associated FTO. *Nat. Chem. Biol.* 7 (12), 885–887. doi:10.1038/nchembio.687
- Ke, S., Pandya-Jones, A., Saito, Y., Fak, J. J., Vågbo, C. B., Geula, S., et al. (2017). m⁶A mRNA Modifications Are Deposited in Nascent Pre-mRNA and Are Not Required for Splicing but Do Specify Cytoplasmic Turnover. *Genes Dev.* 31 (10), 990–1006. doi:10.1101/gad.301036.117
- Kohn, A. D., and Moon, R. T. (2005). Wnt and Calcium Signaling: B-Catenin-independent Pathways. *Cell Calcium* 38 (3-4), 439–446. doi:10.1016/j.ceca.2005.06.022
- Langmead, B., and Salzberg, S. L. (2012). Fast Gapped-Read Alignment with Bowtie 2. *Nat. Methods.* 9 (4), 357–359. doi:10.1038/nmeth.1923
- Li, H. B., H.-B., Tong, J., Zhu, S., Batista, P. J., Duffy, E. E., Zhao, J., et al. (2017). m⁶A mRNA Methylation Controls T Cell Homeostasis by Targeting the IL-7/STAT5/SOCS Pathways. *Nature* 548 (7667), 338–342. doi:10.1038/nature23450
- Li, H., Handsaker, B., Wysoker, A., Fennell, T., Ruan, J., Homer, N., et al. (2009). The Sequence Alignment/Map Format and SAMtools. *Bioinformatics* 25 (16), 2078–2079. doi:10.1093/bioinformatics/btp352

- Li, Y., Xia, L., Tan, K., Ye, X., Zuo, Z., Li, M., et al. (2020). N6-Methyladenosine Co-transcriptionally Directs the Demethylation of Histone H3K9me2. *Nat. Genet.* 52 (9), 870–877. doi:10.1038/s41588-020-0677-3
- Li, Z., Qian, P., Shao, W., Shi, H., He, X. C., Gogol, M., et al. (2018). Suppression of m⁶A Reader Ythdf2 Promotes Hematopoietic Stem Cell Expansion. *Cell Res.* 28 (9), 904–917. doi:10.1038/s41422-018-0072-0
- Li, Z., Weng, H., Su, R., Weng, X., Zuo, Z., Li, C., et al. (2017). FTO Plays an Oncogenic Role in Acute Myeloid Leukemia as a N⁶-Methyladenosine RNA Demethylase. *Cancer Cell* 31 (1), 127–141. doi:10.1016/j.ccell.2016.11.017
- Liao, Y., Smyth, G. K., and Shi, W. (2014). FeatureCounts: An Efficient General Purpose Program for Assigning Sequence Reads to Genomic Features. *Bioinformatics* 30 (7), 923–930. doi:10.1093/bioinformatics/btt656
- Liu, J. E., Li, K., Cai, J., Zhang, M., Zhang, X., Xiong, X., et al. (2020). Landscape and Regulation of m⁶A and m⁶Am Methylome across Human and Mouse Tissues. *Mol. Cell* 77 (2), 426–440. doi:10.1016/j.molcel.2019.09.032
- Liu, J. J., Gao, M., He, J., Wu, K., Lin, S., Jin, L., et al. (2021). The RNA m⁶A Reader YTHDC1 Silences Retrotransposons and Guards ES Cell Identity. *Nature* 591 (7849), 322–326. doi:10.1038/s41586-021-03313-9
- Liu, J., Yue, Y., Han, D., Wang, X., Fu, Y., Zhang, L., et al. (2014). A METTL3-METTL14 Complex Mediates Mammalian Nuclear RNA N6-Adenosine Methylation. *Nat. Chem. Biol.* 10 (2), 93–95. doi:10.1038/nchembio.1432
- Liu, X. X., Wang, H., Zhao, X., Luo, Q., Wang, Q., Tan, K., et al. (2021). Arginine Methylation of METTL14 Promotes RNA N6-Methyladenosine Modification and Endoderm Differentiation of Mouse Embryonic Stem Cells. *Nat. Commun.* 12 (1), 3780. doi:10.1038/s41467-021-24035-6
- Ma, J. Z., Yang, F., Zhou, C. C., Liu, F., Yuan, J. H., Wang, F., et al. (2016). METTL14 Suppresses the Metastatic Potential of Hepatocellular Carcinoma by Modulating N⁶-methyladenosine-dependent Primary MicroRNA Processing. *Hepatology* 65 (2), 529–543. doi:10.1002/hep.28885
- MacDonald, B. T., Tamai, K., and He, X. (2009). Wnt/β-Catenin Signaling: Components, Mechanisms, and Diseases. *Dev. Cell* 17 (1), 9–26. doi:10.1016/j.devcel.2009.06.016
- Mathiyalagan, P., Adamiak, M., Mayourian, J., Sassi, Y., Liang, Y., Agarwal, N., et al. (2019). FTO-dependent N⁶-Methyladenosine Regulates Cardiac Function during Remodeling and Repair. *Circulation* 139 (4), 518–532. doi:10.1161/CIRCULATIONAHA.118.033794
- Meyer, K. D., Patil, D. P., Zhou, J., Zinoviev, A., Skabkin, M. A., Elemento, O., et al. (2015). 5' UTR m⁶A Promotes Cap-independent Translation. *Cell* 163 (4), 999–1010. doi:10.1016/j.cell.2015.10.012
- Mitropoulos, K., Merkouri Papadima, E., Xiromerisiou, G., Balasopoulou, A., Charalampidou, K., Galani, V., et al. (2017). Genomic Variants in the FTO Gene Are Associated with Sporadic Amyotrophic Lateral Sclerosis in Greek Patients. *Hum. Genomics* 11 (1), 30. doi:10.1186/s40246-017-0126-2
- Miyoshi, J., Bobe, A. M., Miyoshi, S., Huang, Y., Hubert, N., Delmont, T. O., et al. (2017). Peripartum Antibiotics Promote Gut Dysbiosis, Loss of Immune Tolerance, and Inflammatory Bowel Disease in Genetically Prone Offspring. *Cell Rep.* 20 (2), 491–504. doi:10.1016/j.celrep.2017.06.060
- Perte, M., Kim, D., Perte, G. M., Leek, J. T., and Salzberg, S. L. (2016). Transcript-level Expression Analysis of RNA-Seq Experiments with HISAT, StringTie and Ballgown. *Nat. Protoc.* 11 (9), 1650–1667. doi:10.1038/nprot.2016.095
- Reya, T., and Clevers, H. (2005). Wnt Signalling in Stem Cells and Cancer. *Nature* 434 (7035), 843–850. doi:10.1038/nature03319
- Roundtree, I. A., Evans, M. E., Pan, T., and He, C. (2017). Dynamic RNA Modifications in Gene Expression Regulation. *Cell* 169 (7), 1187–1200. doi:10.1016/j.cell.2017.05.045
- Sampson, T. R., Debelius, J. W., Thron, T., Janssen, S., Shastri, G. G., Ilhan, Z. E., et al. (2016). Gut Microbiota Regulate Motor Deficits and Neuroinflammation in a Model of Parkinson's Disease. *Cell* 167 (6), 1469–1480. doi:10.1016/j.cell.2016.11.018
- Seki, D., Mayer, M., Hausmann, B., Pjevac, P., Giordano, V., Goeral, K., et al. (2021). Aberrant Gut-Microbiota-Immune-Brain axis Development in Premature Neonates with Brain Damage. *Cell Host Microbe* 29 (10), 1558–1572. doi:10.1016/j.chom.2021.08.004
- Shalem, O., Sanjana, N. E., Hartenian, E., Shi, X., Scott, D. A., Mikkelsen, T. S., et al. (2014). Genome-Scale CRISPR-Cas9 Knockout Screening in Human Cells. *Science* 343 (6166), 84–87. doi:10.1126/science.1247005
- Shi, H., Wang, X., Lu, Z., Zhao, B. S., Ma, H., Hsu, P. J., et al. (2017). YTHDF3 Facilitates Translation and Decay of N(6)-Methyladenosine-Modified RNA. *Cell Res.* 27 (3), 315–328. doi:10.1038/cr.2017.15
- Shu, X., Cao, J., Cheng, M., Xiang, S., Gao, M., Li, T., et al. (2020). A Metabolic Labeling Method Detects m⁶A Transcriptome-wide at Single Base Resolution. *Nat. Chem. Biol.* 16 (8), 887–895. doi:10.1038/s41589-020-0526-9
- Su, R., Dong, L., Li, C., Nachtergaele, S., Wunderlich, M., Qing, Y., et al. (2018). R-2HG Exhibits Anti-tumor Activity by Targeting FTO/m⁶A/MYC/CBPBA Signaling. *Cell* 172 (1–2), 90–105. doi:10.1016/j.cell.2017.11.031
- Su, R., Dong, L., Li, Y., Gao, M., Han, L., Wunderlich, M., et al. (2020). Targeting FTO Suppresses Cancer Stem Cell Maintenance and Immune Evasion. *Cancer Cell* 38 (1), 79–96. doi:10.1016/j.ccell.2020.04.017
- Uddin, M. B., Wang, Z., and Yang, C. (2021). The m⁶A RNA Methylation Regulates Oncogenic Signaling Pathways Driving Cell Malignant Transformation and Carcinogenesis. *Mol. Cancer.* 20 (1), 61. doi:10.1186/s12943-021-01356-0
- Vu, L. P., Pickering, B. F., Cheng, Y., Zaccara, S., Nguyen, D., Minuesa, G., et al. (2017). The N6-Methyladenosine (m⁶A)-Forming Enzyme METTL3 Controls Myeloid Differentiation of Normal Hematopoietic and Leukemia Cells. *Nat. Med.* 23 (11), 1369–1376. doi:10.1038/nm.4416
- Vuong, H. E., Pronovost, G. N., Williams, D. W., Coley, E. J. L., Siegler, E. L., Qiu, A., et al. (2020). The Maternal Microbiome Modulates Fetal Neurodevelopment in Mice. *Nature* 586 (7828), 281–286. doi:10.1038/s41586-020-2745-3
- Wang, X., Li, Y., Chen, W., Shi, H., Eren, A. M., Morozov, A., et al. (2019). Transcriptome-wide Reprogramming of N6-Methyladenosine Modification by the Mouse Microbiome. *Cell Res.* 29 (2), 167–170. doi:10.1038/s41422-018-0127-2
- Wang, X., Lu, Z., Gomez, A., Hon, G. C., Yue, Y., Han, D., et al. (2014). N6-methyladenosine-dependent Regulation of Messenger RNA Stability. *Nature* 505 (7481), 117–120. doi:10.1038/nature12730
- Wang, X., Zhao, B. S., Roundtree, I. A., Lu, Z., Han, D., Ma, H., et al. (2015). N6-methyladenosine Modulates Messenger RNA Translation Efficiency. *Cell* 161 (6), 1388–1399. doi:10.1016/j.cell.2015.05.014
- Wang, Y., Li, Y., Toth, J. I., Petroski, M. D., Zhang, Z., and Zhao, J. C. (2014). N6-methyladenosine Modification Destabilizes Developmental Regulators in Embryonic Stem Cells. *Nat. Cell Biol.* 16 (2), 191–198. doi:10.1038/ncb2902
- Wang, Y., Li, Y., Yue, M., Wang, J., Kumar, S., Wechsler-Reya, R. J., et al. (2018). N6-methyladenosine RNA Modification Regulates Embryonic Neural Stem Cell Self-Renewal through Histone Modifications. *Nat. Neurosci.* 21 (2), 195–206. doi:10.1038/s41593-017-0057-1
- Willyard, C. (2021). How Gut Microbes Could Drive Brain Disorders. *Nature* 590 (7844), 22–25. doi:10.1038/d41586-021-00260-3
- Wu, J., Wang, K., Wang, X., Pang, Y., and Jiang, C. (2021). The Role of the Gut Microbiome and its Metabolites in Metabolic Diseases. *Protein Cell* 12 (5), 360–373. doi:10.1007/s13238-020-00814-7
- Wu, Q., Liang, X., Wang, K., Lin, J., Wang, X., Wang, P., et al. (2021). Intestinal Hypoxia-Inducible Factor 2α Regulates Lactate Levels to Shape the Gut Microbiome and Alter Thermogenesis. *Cell Metab.* 33 (10), 1988–2003. doi:10.1016/j.cmet.2021.07.007
- Wu, T., Hu, E., Xu, S., Chen, M., Guo, P., Dai, Z., et al. (2021). ClusterProfiler 4.0: A Universal Enrichment Tool for Interpreting Omics Data. *Innovation* 2 (3), 100141. doi:10.1016/j.xinn.2021.100141
- Xiao, S., Cao, S., Huang, Q., Xia, L., Deng, M., Yang, M., et al. (2019). The RNA N6-Methyladenosine Modification Landscape of Human Fetal Tissues. *Nat. Cell Biol.* 21 (5), 651–661. doi:10.1038/s41556-019-0315-4
- Xiao, W., Adhikari, S., Dahal, U., Chen, Y.-S., Hao, Y.-J., Sun, B.-F., et al. (2016). Nuclear m⁶A Reader YTHDC1 Regulates mRNA Splicing. *Mol. Cell* 61 (4), 507–519. doi:10.1016/j.molcel.2016.01.012
- Yoon, K.-J., Ringeling, F. R., Vissers, C., Jacob, F., Pokrass, M., Jimenez-Cyrus, D., et al. (2017). Temporal Control of Mammalian Cortical Neurogenesis by m⁶A Methylation. *Cell* 171 (4), 877–889. doi:10.1016/j.cell.2017.09.003
- Zhang, X., Chen, B.-d., Zhao, L.-d., and Li, H. (2020). The Gut Microbiota: Emerging Evidence in Autoimmune Diseases. *Trends Mol. Med.* 26 (9), 862–873. doi:10.1016/j.molmed.2020.04.001
- Zhao, B. S., Roundtree, I. A., and He, C. (2017a). Post-transcriptional Gene Regulation by mRNA Modifications. *Nat. Rev. Mol. Cell Biol.* 18 (1), 31–42. doi:10.1038/nrm.2016.132
- Zhao, B. S., Wang, X., Beadell, A. V., Lu, Z., Shi, H., Kuuspalu, A., et al. (2017b). m⁶A-dependent Maternal mRNA Clearance Facilitates Zebrafish Maternal-To-Zygotic Transition. *Nature* 542 (7642), 475–478. doi:10.1038/nature21355

- Zheng, G., Dahl, J. A., Niu, Y., Fedorcsak, P., Huang, C.-M., Li, C. J., et al. (2013). ALKBH5 Is a Mammalian RNA Demethylase that Impacts RNA Metabolism and Mouse Fertility. *Mol. Cell* 49 (1), 18–29. doi:10.1016/j.molcel.2012.10.015
- Zhou, J., Wan, J., Gao, X., Zhang, X., Jaffrey, S. R., and Qian, S.-B. (2015). Dynamic m⁶A mRNA Methylation Directs Translational Control of Heat Shock Response. *Nature* 526 (7574), 591–594. doi:10.1038/nature15377

Conflict of Interest: The authors declare that the research was conducted in the absence of any commercial or financial relationships that could be construed as a potential conflict of interest.

Publisher's Note: All claims expressed in this article are solely those of the authors and do not necessarily represent those of their affiliated organizations, or those of the publisher, the editors, and the reviewers. Any product that may be evaluated in this article, or claim that may be made by its manufacturer, is not guaranteed or endorsed by the publisher.

Copyright © 2022 Xiao, Liu, Li, Cui, Wang, Wang, Ren, Xia, Wang and Li. This is an open-access article distributed under the terms of the Creative Commons Attribution License (CC BY). The use, distribution or reproduction in other forums is permitted, provided the original author(s) and the copyright owner(s) are credited and that the original publication in this journal is cited, in accordance with accepted academic practice. No use, distribution or reproduction is permitted which does not comply with these terms.